Mahdi Takaffoli
Department of Mechanical Engineering,
Massachusetts Institute of Technology,
Cambridge, MA 02139

Teng Zhang[1]
Department of Mechanical Engineering,
Massachusetts Institute of Technology,
Cambridge, MA 02139

David Parks
Department of Mechanical Engineering,
Massachusetts Institute of Technology,
Cambridge, MA 02139

Xuanhe Zhao[2]
Department of Mechanical Engineering,
Massachusetts Institute of Technology,
Cambridge, MA 02139;
Department of Civil and
Environmental Engineering,
Massachusetts Institute of Technology,
Cambridge, MA 02139
e-mail: zhaox@mit.edu

Mechanochemically Responsive Viscoelastic Elastomers

Mechanochemically responsive (MCR) polymers have been designed to possess unconventional properties such as changing colors, self-healing, and releasing catalysts under deformation. These properties of MCR polymers stem from a class of molecules, referred to as mechanophores, whose chemical reactions can be controlled by mechanical forces. Although extensive studies have been devoted to the syntheses of MCR polymers by incorporating various mechanophores into polymer networks, the intricate interactions between mechanical forces and chemical reactions in MCR polymers across multiple length and time scales are still not well understood. In this paper, we focus on mechanochemical responses in viscoelastic elastomers and develop a theoretical model to characterize the coupling between viscoelasticity and chemical reactions of MCR elastomers. We show that the kinetics of viscoelasticity and mechanophore reactions introduce different time scales into the MCR elastomers. The model can consistently represent experimental data on both mechanical properties and chemical reactions of MCR viscoelastic elastomers. In particular, we explain recent experimental observations on the increasing chemical activation during stress relaxation of MCR elastomers, which cannot be explained with existing models. The proposed model provides a theoretical foundation for the design of future MCR polymers with desirable properties.
[DOI: 10.1115/1.4033431]

1 Introduction

Mechanical forces applied on molecules can manipulate their covalent bonds and trigger chemical reactions [1–5]. This phenomenon is commonly referred to as a mechanochemical reaction, and the molecules capable of selective mechanochemical reactions as mechanophores [6]. In recent years, mechanophores have been widely explored in the design of new materials. One strategy commonly employed in such designs is to covalently couple mechanophores on polymer networks to achieve MCR polymers—a new type of multifunctional and responsive polymers [7–9]. Deformation of MCR polymers applies mechanical forces on mechanophores and controls their mechanochemical reactions. The development of new mechanophores and polymer networks have led to various MCR polymers that possess extraordinary properties and functions such as self-healing [10,11], color-changing, and fluorescence-varying [12,13], catalyst-releasing [4] or force-controlled cross-linking [14].

In particular, elastomers were recently adopted as matrices for mechanophores, owning to their capability of large and elastic deformations [15–21]. The resultant MCR elastomers can undergo multiple cycles of reversible deformations and repeated mechanochemical reactions, in contrast to permanent deformation or fracture of glassy polymers, creating new potentials for building flexible MCR devices with various applications in flexible displays, optoelectronics, biomedical luminescent devices, and camouflage skins [22].

In contrast to the extensive efforts devoted to syntheses of MCR polymers, very few models have been developed to reveal intricate interplays between mechanical forces and chemical reactions in MCR polymers. Recently, elastic and viscoelastic models for MCR glassy polymers [23] and elastomers [24,25] have been reported. While these models are consistent with some experimental data, they fail to explain other important experimental phenomena. For example, existing models cannot account for the increasing chemical activation of MCR polymers undergoing stress–relaxation tests [25]. In addition, rapid accumulation of experimental data in the field demands the development of general models that can systematically characterize the interactions between viscoelastic deformations and mechanochemical reactions observed in different experiments—analogous to the development of generalized Maxwell models for viscoelastic materials.

In the current paper, we aim at developing a simple yet general theoretical model to investigate the interactions between strain-rate-dependent behaviors of viscoelastic elastomers and mechanochemical reactions of the embedded mechanophores. In Sec. 2, we will present the fundamental assumptions and formulations of the model, which consists of a generalized Maxwell model with nonlinear springs and dashpots coupled with modules of mechanophores. Section 3 discusses typical features of the proposed model, including the chemical activation, of a single relaxable network, and combined elastic and relaxable networks. Using the developed simple model, we will reveal different modes of interactions between viscoelasticity and reactions in MCR elastomers across multiple time scales. In Sec. 4, we apply the model to characterize the recent experimental measurements on viscoelasticity and mechanochemical reactions of MCR elastomers. In particular, we will explain recent experimental observations on the increasing chemical activation of MCR elastomers during stress–relaxation process. Concluding remarks are made in Sec. 5.

2 Formulation of the Model

We aim to develop a simple thermodynamic-based model for MCR viscoelastic elastomers to account for the interactions between viscoelasticity and mechanochemical reactions in the elastomers. Since the sizes of mechanophores are usually much smaller than the lengths of polymer chains, and the concentration of mechanophores in the elastomers is very small, e.g., less than 1 wt.% [16,22], it is commonly assumed that the presence of mechanophores does not affect the mechanical properties of the elastomers [24,25]. Based on this assumption, we will first

[1]Present address: Department of Mechanical and Aerospace Engineering, Syracuse University, Syracuse, NY 13244.
[2]Corresponding author.
Contributed by the Applied Mechanics Division of ASME for publication in the Journal of Applied Mechanics. Manuscript received March 6, 2016; final manuscript received April 12, 2016; published online May 9, 2016. Editor: Yonggang Huang.

formulate a thermodynamic model for viscoelastic behaviors of the elastomer, and then couple mechanophores into the model to study their mechanochemical reactions in viscoelastic elastomers.

2.1 Nonequilibrium Thermodynamics of a Viscoelastic Elastomer. To focus on the key physical features of viscoelasticity, we consider a piece of viscoelastic elastomer under homogeneous deformation at a constant temperature [26]. At the reference (undeformed) state, the elastomer has dimensions L_1, L_2, and L_3 (Fig. 1(*a*)). At the current state, the elastomer is subjected to forces P_1, P_2, and P_3 along three orthogonal directions, and its dimensions change to l_1, l_2, and l_3 (Fig. 1(*b*)). As the dimensions of the elastomer vary infinitesimally by δl_1, δl_2, and δl_3, the mechanical forces do work by $P_1\delta l_1 + P_2\delta l_2 + P_3\delta l_3$. Thermodynamics requires that the increase in the free energy of the elastomer should not exceed the total work done on it, i.e.,

$$\delta F \le P_1\delta l_1 + P_2\delta l_2 + P_3\delta l_3 \tag{1}$$

where F is the Helmholtz free energy of the elastomer. It should be noted that the small changes in Eq. (1) are time directed, such that δx means the change of the quantity x from a specific time t to a slightly later time $t + \delta t$.

At the current state, the principal stretches of the elastomer can be calculated as $\lambda_1 = l_1/L_1$, $\lambda_2 = l_2/L_2$, and $\lambda_3 = l_3/L_3$ and the principal nominal stresses as $s_1 = P_1/(L_2L_3)$, $s_2 = P_2/(L_1L_3)$, and $s_3 = P_3/(L_1L_2)$. Defining Helmholtz free-energy density of the elastomer as $W = F/(L_1L_2L_3)$, we can further express the thermodynamic inequality (Eq. (1)) as

$$\delta W \le s_1\delta\lambda_1 + s_2\delta\lambda_2 + s_3\delta\lambda_3 \tag{2}$$

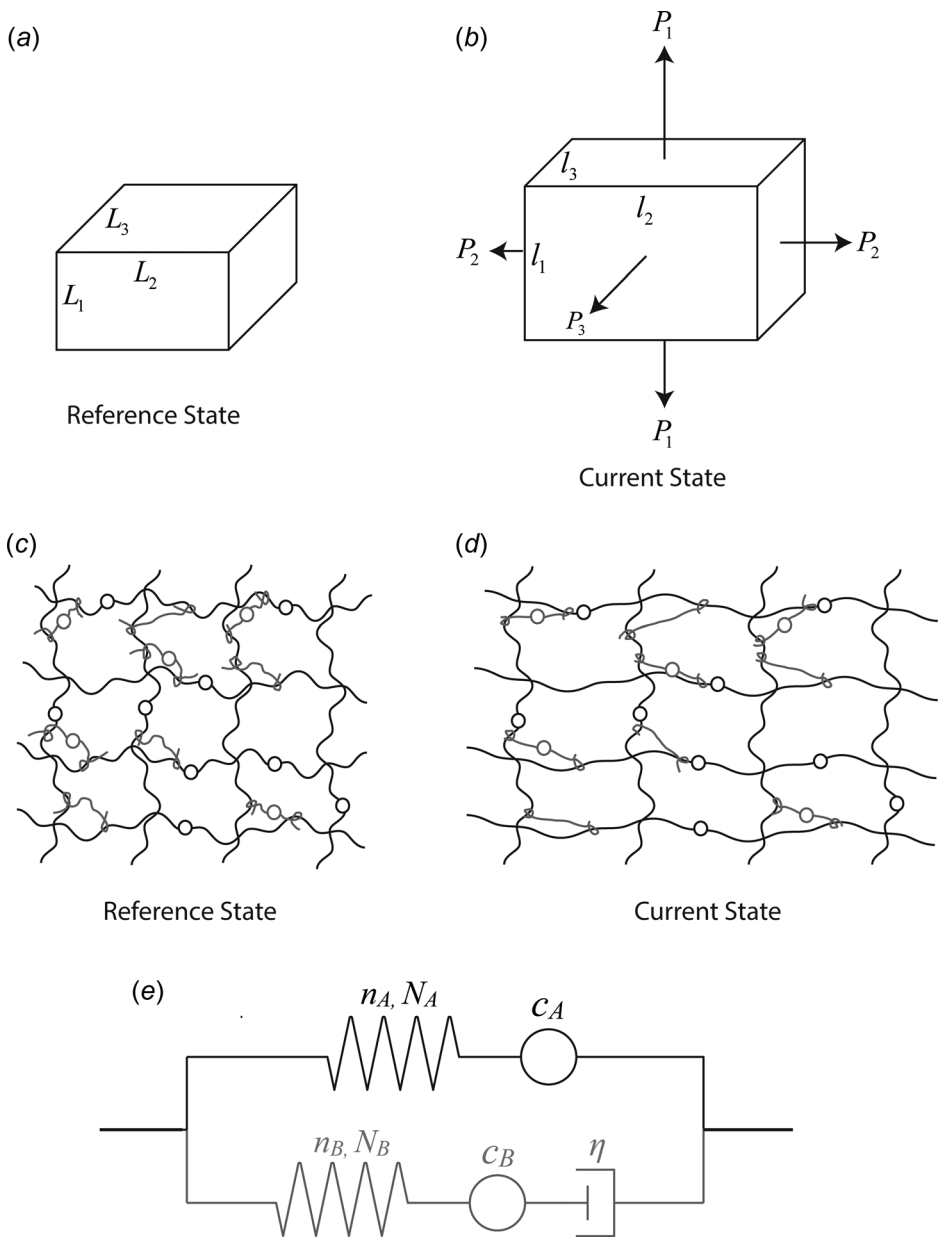

Fig. 1 A piece of a viscoelastic elastomer in the undeformed reference state (*a*) and in the deformed current state (*b*). Schematics of the polymer network of a MCR viscoelastic elastomer in the reference (*c*) and current (*d*) states. The elastomer consists of pure elastic (black) and relaxable chains (gray). (*e*) A schematic of a generalized Maxwell model coupled with modules of mechanophores.

As a model of the viscoelastic elastomer, the free-energy density function of the elastomer is assumed to be prescribed as a function

$$W = W(\lambda_1, \lambda_2, \lambda_3, \Lambda^v) \tag{3}$$

where Λ^v is a dimensionless internal variable associated with the dissipative process of the viscoelastic elastomer. As the variables in Eq. (3) change by infinitesimal amounts, the free-energy density function varies by

$$\delta W = \frac{\partial W}{\partial \lambda_1}\delta\lambda_1 + \frac{\partial W}{\partial \lambda_2}\delta\lambda_2 + \frac{\partial W}{\partial \lambda_3}\delta\lambda_3 + \frac{\partial W}{\partial \Lambda^v}\delta\Lambda^v \tag{4}$$

Substituting Eq. (4) into Eq. (2), we can rewrite the thermodynamic inequality as

$$\left(\frac{\partial W}{\partial \lambda_1} - s_1\right)\delta\lambda_1 + \left(\frac{\partial W}{\partial \lambda_2} - s_2\right)\delta\lambda_2 + \left(\frac{\partial W}{\partial \lambda_3} - s_3\right)\delta\lambda_3 + \frac{\partial W}{\partial \Lambda^v}\delta\Lambda^v \le 0 \tag{5}$$

To satisfy this inequality, we further assume that the first three terms in Eq. (5) vanish with arbitrary variations of $\delta\lambda_1$, $\delta\lambda_2$, and $\delta\lambda_3$, so that

$$s_1 = \frac{\partial W(\lambda_1, \lambda_2, \lambda_3, \Lambda^v)}{\partial \lambda_1} \tag{6a}$$

$$s_2 = \frac{\partial W(\lambda_1, \lambda_2, \lambda_3, \Lambda^v)}{\partial \lambda_2} \tag{6b}$$

$$s_3 = \frac{\partial W(\lambda_1, \lambda_2, \lambda_3, \Lambda^v)}{\partial \lambda_3} \tag{6c}$$

Therefore, the thermodynamic inequality can be further expressed as

$$\dot{\Lambda}^v \frac{\partial W(\lambda_1, \lambda_2, \lambda_3, \Lambda^v)}{\partial \Lambda^v} \le 0 \tag{7}$$

where $\dot{\Lambda}^v = \delta\Lambda^v/\delta t$ is the time derivative of the internal variable. Equations (6) and (7) must hold at every point of the elastomer and for all times during a deformation process. To capture the main physical features of viscoelasticity, we adopt a simple evolution law for Λ^v that satisfies Eq. (7), i.e.

$$\dot{\Lambda}^v = -\frac{1}{\eta}\frac{\partial W(\lambda_1, \lambda_2, \lambda_3, \Lambda^v)}{\partial \Lambda^v} \tag{8}$$

where η is a positive number with the dimension of viscosity (i.e., Pa · s).

2.2 Free-Energy Density Function of a Viscoelastic Elastomer.

Adopting a generalized Maxwell model [27,28], we assume that the viscoelastic behavior of the elastomer can be attributed to two polymer networks acting in parallel as indicated in Figs. 1(*c*) and 1(*d*) for the reference and current states, respectively [27,29–31]. The first network (i.e., network *A*) is a purely elastic network that characterizes the time-independent mechanical behavior of the elastomer using a nonlinear spring; and the second network (i.e., network *B*) is a relaxable network that accounts for the time-dependent mechanical behavior of the elastomer using a nonlinear spring and a dashpot in series. (Note that mechanophores will be coupled onto these networks in Sec. 2.5.)

Based on the model illustrated in Fig. 1(*e*) and the affine-network assumption [32,33], polymer chains in network *A* and *B* will have the same stretch

$$\Lambda = \frac{r}{r_0} \tag{9}$$

where r_0 and r are the end-to-end distance of a polymer chain at reference and current states, respectively. While the stretch of polymer chains in network *A* is elastic, the stretch of polymer chains in network *B* can be decomposed into an elastic part Λ^e and an inelastic part Λ^v for the elastomer under deformation illustrated in Fig. 1(*a*), i.e.

$$\Lambda = \Lambda^e\Lambda^v \tag{10}$$

where Λ^v is also the internal variable to characterize the dissipative process in Eq. (8).

Therefore, we can express the Helmholtz free-energy density function of the elastomer (Fig. 1(*b*)) as

$$W = W_A(\Lambda) + W_B(\Lambda^e) \tag{11}$$

where W_A and W_B are the Helmholtz free-energy density functions of networks *A* and *B* at the current state per unit volume of the elastomer at the reference state, respectively; and $\Lambda^e = \Lambda/\Lambda^v$ based on Eq. (10).

Since the type of polymers in networks *A* and *B* is the same, the polymer chains in both networks have the same Kuhn monomer length *b*. We further denote the number of Kuhn monomers of a polymer chain in networks *A* and *B* as n_A and n_B, respectively. Adopting the Langevin model [34,35], we can express the free energy of a stretched polymer chain in network *A* as

$$w_A = n_A kT\left(\frac{\beta_A}{\tanh\beta_A} + \ln\frac{\beta_A}{\sinh\beta_A}\right) \tag{12}$$

where $\beta_A = L^{-1}(\Lambda/\sqrt{n_A})$ is the inverse Langevin function of $\Lambda/\sqrt{n_A}$, where Langevin function is defined as $L(x) = \coth(x) - 1/x$; *k* is the Boltzmann constant; and *T* is the absolute temperature in Kelvin. The free energy of a stretched polymer chain in network *B* is expressed as

$$w_B = n_B kT\left(\frac{\beta_B}{\tanh\beta_B} + \ln\frac{\beta_B}{\sinh\beta_B}\right) \tag{13}$$

where $\beta_B = L^{-1}(\Lambda^e/\sqrt{n_B})$ and $\Lambda^e = \Lambda/\Lambda^v$ from Eq. (10).

The numbers of polymer chains in networks *A* and *B* per unit volume of the elastomer at the reference state are denoted as N_A and N_B, respectively. Further taking the elastomer as incompressible, i.e., $\lambda_1 * \lambda_2 * \lambda_3 = 1$, we can explicitly express the free-energy density function of the elastomer as

$$W = N_A n_A kT\left(\frac{\beta_A}{\tanh\beta_A} + \ln\frac{\beta_A}{\sinh\beta_A}\right) + N_B n_B kT\left(\frac{\beta_B}{\tanh\beta_B} + \ln\frac{\beta_B}{\sinh\beta_B}\right) - p(\lambda_1\,\lambda_2\,\lambda_3 - 1) \tag{14}$$

where the scalar *p* acts as a Lagrange multiplier to enforce the incompressibility of the elastomer and is calculated from the equilibrium equations and boundary conditions.

In order to relate the stretch of polymer chains to macroscopic principal stretches of the elastomer, we assume both networks follow the eight-chain network model [36], so that

$$\Lambda = \sqrt{\frac{\lambda_1^2 + \lambda_2^2 + \lambda_3^2}{3}} \tag{15}$$

According to Eqs. (6), (14), and (15), we can now calculate the principal nominal stresses in the elastomer as

$$s_1 = \frac{\lambda_1 kT}{3\Lambda}\left(N_A\sqrt{n_A}\beta_A + \frac{N_B\sqrt{n_B}\beta_B}{\Lambda^v}\right) - p\lambda_2\lambda_3 \tag{16a}$$

$$s_2 = \frac{\lambda_2 kT}{3\Lambda}\left(N_A\sqrt{n_A}\beta_A + \frac{N_B\sqrt{n_B}\beta_B}{\Lambda^v}\right) - p\lambda_1\lambda_3 \tag{16b}$$

$$s_3 = \frac{\lambda_3 kT}{3\Lambda}\left(N_A\sqrt{n_A}\beta_A + \frac{N_B\sqrt{n_B}\beta_B}{\Lambda^v}\right) - p\lambda_1\lambda_2 \tag{16c}$$

And, therefore, the principal Cauchy stresses as

$$\sigma_1 = \lambda_1 s_1 = \frac{\lambda_1^2 kT}{3\Lambda}\left(N_A\sqrt{n_A}\beta_A + \frac{N_B\sqrt{n_B}\beta_B}{\Lambda^v}\right) - p \tag{17a}$$

$$\sigma_2 = \lambda_2 s_2 = \frac{\lambda_2^2 kT}{3\Lambda}\left(N_A\sqrt{n_A}\beta_A + \frac{N_B\sqrt{n_B}\beta_B}{\Lambda^v}\right) - p \tag{17b}$$

$$\sigma_3 = \lambda_3 s_3 = \frac{\lambda_3^2 kT}{3\Lambda}\left(N_A\sqrt{n_A}\beta_A + \frac{N_B\sqrt{n_B}\beta_B}{\Lambda^v}\right) - p \tag{17c}$$

According to Eqs. (8) and (14), we can further calculate the evolution law of the internal variable Λ^v as

$$\dot{\Lambda}^v = \left(\frac{1}{\eta}N_B\sqrt{n_B}kT\right)\frac{\Lambda}{(\Lambda^v)^2}\beta_B \quad \text{with} \quad \Lambda^v|_{t=0} = 1 \tag{18}$$

It is evident that η represents the viscosity of the dashpot in the model of Fig. 1(*e*).

Solving Eqs. (17) and (18) together with initial and boundary conditions can provide the evolution of stresses, deformations, and dissipation in the viscoelastic elastomer over time.

2.3 Mechanochemical Reaction of Mechanophores. Now that a thermodynamic model of viscoelastic elastomers has been established, we will study the effects of elastomer deformation and polymer chain forces on reactions of mechanophores as illustrated in Fig. 1(*e*). It should be noted that since the contribution of mechanophores to the free energy of elastomer is negligible, they are not included in the current thermodynamic model of viscoelastic elastomers. While this treatment significantly simplifies our model, the contribution of mechanophores to free-energy variation of elastomers can be incorporated in future models based on the nonequilibrium thermodynamic framework presented in Sec. 2.1.

In order to compare our model with experimental data in Sec. 4, we will discuss the mechanochemical reaction based on a specific mechanophore, spiropyran, which has been widely used in MCR elastomers. However, the framework of the theory is applicable to other types of mechanophores. Mechanochemical reaction or transformation of a mechanophore among different states accompanies with the change of potential energy of the molecule along a reaction coordinate [37]. Colorless spiropyran is able to transform into a colored state, merocyanine, through a reversible ring-opening reaction (Fig. 2(*a*)), following a potential energy profile on the reaction coordinate (Fig. 2(*b*)). The potential energy profile is significantly affected by the forces applied on the molecule as shown in Fig. 2(*c*) [15]. We denote the numbers of mechanophores coupled to elastic and relaxable networks per unit volume of elastomer as c_A and c_B, respectively. Specifically, the numbers of spiropyran on elastic and relaxable networks per unit volume of elastomer are denoted as c_A^S and c_B^S, respectively; and the numbers of merocyanine coupled to elastic and relaxable networks per unit volume of elastomer as c_A^M and c_B^M, respectively. It is evident that $c_A = c_A^M + c_A^S$ and $c_B = c_B^M + c_B^S$. Mechanophore transformation between the two states of spiropyran and merocyanine is governed by the following kinetic relations for networks A and B [38]:

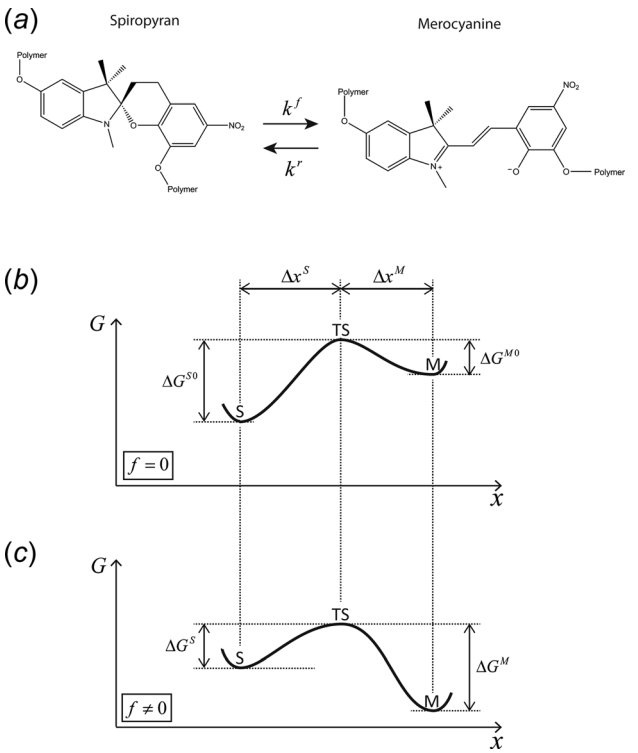

Fig. 2 Mechanochemical transformation of a mechanophore molecule through a reversible ring-opening reaction from the spiropyran state to the merocyanine state (*a*). Potential energy landscapes of the mechanophore under zero (*b*) and nonzero (*c*) applied force.

$$\frac{dc_A^M}{dt} = k_A^f c_A^S - k_A^r c_A^M \tag{19a}$$

$$\frac{dc_B^M}{dt} = k_B^f c_B^S - k_B^r c_B^M \tag{19b}$$

where k_A^f and k_A^r represent force-dependent forward (spiropyran to merocyanine) and reverse (merocyanine to spiropyran) reaction rates of mechanophores coupled to the elastic network, respectively; and k_B^f and k_B^r represent force-dependent forward and reverse reaction rates of mechanophores coupled to the relaxable network, respectively. The unit of all reaction rates k_A^f, k_A^r, k_B^f, and k_B^r is s^{-1}. As the number of merocyanine in the MCR elastomer determines its color and fluorescence, we will focus on the merocyanine concentration during mechanochemical reactions. Since c_A and c_B remain constant during reactions, Eq. (19) can be rewritten as

$$\frac{dc_A^M}{dt} = -\left(k_A^f + k_A^r\right)c_A^M + k_A^f c_A \tag{20a}$$

$$\frac{dc_B^M}{dt} = -\left(k_B^f + k_B^r\right)c_B^M + k_B^f c_B \tag{20b}$$

The above ordinary differential equations can be solved, given the reaction rates and initial conditions $c_A^M|_{t=0}$ and $c_B^M|_{t=0}$. After solving Eq. (20), the total number of merocyanine in a unit volume of the MCR elastomer c^M can be calculated as

$$c^M(t) = c_A^M(t) + c_B^M(t) \tag{21}$$

We can further define the activation efficiency of mechanophores as

$$\alpha_A(t) = \frac{c_A^M(t)}{c_A} \tag{22a}$$

$$\alpha_B(t) = \frac{c_B^M(t)}{c_B} \tag{22b}$$

$$\alpha(t) = \frac{c_A^M(t) + c_B^M(t)}{c_A + c_B} = \frac{c_A}{c_A + c_B}\alpha_A(t) + \frac{c_B}{c_A + c_B}\alpha_B(t) \tag{22c}$$

for network A, network B, and the elastomer, respectively.

When the mechanochemical reactions of mechanophores reach equilibrium, the number of merocyanine per unit volume of elastomer can be calculated based on Eq. (20) as

$$c_A^M\Big|_{\text{equ}} = c_A \frac{k_A^f}{k_A^f + k_A^r} \tag{23a}$$

$$c_B^M\Big|_{\text{equ}} = c_B \frac{k_B^f}{k_B^f + k_B^r} \tag{23b}$$

By substituting Eq. (23) into Eq. (22), we can calculate the activation efficiency at equilibrium as

$$\alpha_A\Big|_{\text{equ}} = \frac{k_A^f}{k_A^f + k_A^r} \tag{24a}$$

$$\alpha_B\Big|_{\text{equ}} = \frac{k_B^f}{k_B^f + k_B^r} \tag{24b}$$

$$\alpha\Big|_{\text{equ}} = \frac{c_A}{c_A + c_B}\alpha_A\Big|_{\text{equ}} + \frac{c_B}{c_A + c_B}\alpha_B\Big|_{\text{equ}} \tag{24c}$$

2.4 Force-Dependent Reaction Rates of Mechanophores. From Eq. (19), it can be seen that the reaction rates k_A^f, k_A^r, k_B^f, and k_B^r are critical parameters that determine the mechanochemical reactions in MCR elastomers. Following the transition state theory [37], these parameters can be determined by the potential energy profile of the mechanophore (Figs. 2(*b*) and 2(*c*)). Along the reaction pathway, the potential energy of the mechanophore goes from one minimum (the reactant state) to another minimum (the product state) and passes through a transition state. The difference between potential energies of reactant and transition states is the activation energy which is the minimum energy required for the reaction to occur. The force-free forward and reverse activation energies are denoted by ΔG^{S0} and ΔG^{M0}, respectively (Fig. 2(*b*)). Adopting the Arrhenius equation, the activation energies can be related to the force-free reaction rates as [39]

$$k^{f0} = D^f \exp\left(-\frac{\Delta G^{S0}}{kT}\right) \tag{25a}$$

$$k^{r0} = D^r \exp\left(-\frac{\Delta G^{M0}}{kT}\right) \tag{25b}$$

where k^{f0} and k^{r0} are the force-free forward and reverse reaction rates, respectively; and the frequency factors D^f and D^r are related to the diffusion rates of the molecule toward the transition state [40]. Typical values of D^f and D^r are on the order of 10^{13} s^{-1} [41].

Applying force on the mechanophore lowers the activation energy of the forward transformation to ΔG^S and increases the activation energy of the reverse transformation to ΔG^M as illustrated in Fig. 2(*c*). Therefore, the force-dependent forward and reverse reaction rates can be calculated as

$$k^f = D^f \exp\left(-\frac{\Delta G^S}{kT}\right) \tag{26a}$$

$$k^r = D^r \exp\left(-\frac{\Delta G^M}{kT}\right) \tag{26b}$$

According to the Bell model [42], the applied force f linearly modifies the activation energies by

$$\Delta G^S = \Delta G^{S0} - f\Delta x^S \tag{27a}$$

$$\Delta G^M = \Delta G^{M0} + f\Delta x^M \tag{27b}$$

where Δx^S and Δx^M are reaction distances from spiropyran and merocyanine states to the transition state, respectively (Fig. 2(*b*)). Therefore, by substituting Eqs. (25) and (27) into Eq. (26), the force-dependent forward and reverse reaction rates of mechanophores in each network can be expressed as

$$k_A^f = k^{f0} \exp\left(\frac{f_A \Delta x^S}{kT}\right) \tag{28a}$$

$$k_A^r = k^{r0} \exp\left(-\frac{f_A \Delta x^M}{kT}\right) \tag{28b}$$

$$k_B^f = k^{f0} \exp\left(\frac{f_B \Delta x^S}{kT}\right) \tag{28c}$$

$$k_B^r = k^{r0} \exp\left(-\frac{f_B \Delta x^M}{kT}\right) \tag{28d}$$

where f_A and f_B are chain forces in elastic and relaxable networks, respectively. In addition, we can further assume that $\Delta x = \Delta x^M = \Delta x^S$ in Eqs. (27) and (28) based on the results from recent atomistic calculations and experiments [25,41], where the reaction distance Δx was reported to be on the order of a few angstroms.

2.5 Coupling Between Viscoelasticity and Mechanochemical Reactions. The coupling between viscoelastic deformation of MCR elastomers and mechanochemical reactions of mechanophores is through the forces that are generated in the stretched polymer chains of the elastomer and applied on mechanophores (Figs. 1(*c*)–1(*e*)). Here, we have neglected the effects of intermolecular forces on the reaction kinetics of mechanophores since these forces are weak and therefore not included in the thermodynamic model of the elastomer (Sec. 2.2). Furthermore, their effects on the mechanochemical reactions of mechanophores are not well understood [25].

At the reference state, the length of unstretched polymer chains in network A is given from random-walk statistics as $r_{A0} = \sqrt{n_A}b$. From Eq. (9), the length of stretched polymer chains in network A at the current state can be calculated as $r_A = \Lambda\sqrt{n_A}b$. Therefore, from Eq. (12), the force on a polymer chain in network A is

$$f_A = \frac{\partial w_A}{\partial r_A} = \frac{kT}{b} L^{-1}\left(\frac{\Lambda}{\sqrt{n_A}}\right) \tag{29}$$

At the reference state, the length of unstretched polymer chains in network B is given from random-walk statistics as $r_{B0} = \sqrt{n_B}b$. The chains are stretched to a length of $r_B^e = \Lambda^e\sqrt{n_B}b$ due to pure elastic deformation at the current state. From Eq. (13), the force of a polymer chain in network B can be calculated as

$$f_B = \frac{\partial w_B}{\partial r_B^e} = \frac{kT}{b} L^{-1}\left(\frac{\Lambda/\Lambda^v}{\sqrt{n_B}}\right) \tag{30}$$

Solving Eqs. (17) and (18) with initial and boundary conditions will give the macroscopic deformation and stresses in the elastomer and stretches in polymer chains. Subsequently, the chain forces in networks A and B can be calculated with Eqs. (29) and (30). By substituting chain forces into Eq. (28) and subsequently solving Eq. (19), the rates of mechanochemical reactions and activation efficiencies can be calculated.

3 Results and Discussion

3.1 Characteristic Time Scales in MCR Viscoelastic Elastomers. Now that a model for coupled viscoelasticity and mechanochemical reactions in elastomers has been established, we will use the model to discuss the unique features of MCR viscoelastic elastomers. Both viscoelasticity and mechanochemical reactions introduce characteristic time scales into the material. The interplay of these time scales can lead to interesting mechanical and chemical responses of the elastomer over time.

Based on the dashpot in series with the nonlinear spring in network B, we define a typical time scale for mechanical relaxation as [30]

$$\tau^M = \frac{\eta}{N_B kT} \tag{31}$$

where $N_B kT$ is the initial shear modulus of the nonlinear spring in network B [27]. Although τ^M in Eq. (31) does not account for the nonlinearity of the relaxation response, it is still representative of this process over long times when strain and time-dependent effects can be separated [43,44].

For the mechanophore in either network of the model, a typical time scale for mechanochemical reactions can be defined as [24]

$$\tau^R = \frac{1}{k^f + k^r} \tag{32}$$

Since the reaction rate significantly depends on the force applied on the mechanophore and the applied force may vary over time, we further define the time scale for reactions by considering a typical scale of the applied force $\bar{f}$, i.e.

$$\tau^R = \frac{1}{k^{f0}\exp\left(\frac{\bar{f}\Delta x}{kT}\right) + k^{r0}\exp\left(\frac{-\bar{f}\Delta x}{kT}\right)} \tag{33}$$

In an extreme case, when the applied force on the mechanophore is zero, a typical time scale for the force-free reaction is

$$\tau^{R0} = \frac{1}{k^{f0} + k^{r0}} \tag{34}$$

For spiropyran and merocyanine, τ^{R0} is about 20 s, since $k^{f0} = 8.5 \times 10^{-6}\,\mathrm{s}^{-1}$ and $k^{r0} = 4.9 \times 10^{-2}\,\mathrm{s}^{-1}$ according to the recent experiments [41], and the activation efficiency at equilibrium is only 1.7×10^{-4} (Eq. (24)). Applying force on the mechanophore modifies the reaction time scale nonmonotonically [24] and transforms the molecule toward its merocyanine state, i.e., higher activation efficiency. For example, if we take $\Delta x = 2.7 \times 10^{-10}\,\mathrm{m}$ and $T = 300\,\mathrm{K}$ in Eq. (33), an average force of 70 pN applied on the mechanophore increases τ^R to 754 s and raises the activation efficiency to 0.6. If we increase the force to 150 pN, the reaction time scale τ^R reduces to 7 s, and the mechanophore almost fully transforms to the merocyanine state, i.e., $\alpha|_{\mathrm{equ}} \approx 1$.

3.2 Typical Mechanical and Mechanochemical Behaviors. Now that the characteristic time scales in MCR viscoelastic elastomers have been identified, we will discuss typical mechanical and mechanochemical behaviors of the elastomers with different ratios of mechanical to reaction time scales (i.e., different τ^M/τ^R). To focus on the essential physical features, we assume the elastomer undergoes a history of relatively simple deformation: The elastomer is stress free and in equilibrium when $t < 0$ and then subjected to a stretch at $t = 0$, which is maintained constant over time (Fig. 3(*b*)). This is analogous to a stress–relaxation test on viscoelastic materials.

In all calculations, we take $T = 300\,\mathrm{K}$ and typical values of $b = 14.7 \times 10^{-10}\,\mathrm{m}$, $\Delta x = 2.7 \times 10^{-10}\,\mathrm{m}$, $k^{f0} = 8.5 \times 10^{-6}\,\mathrm{s}^{-1}$, and $k^{r0} = 4.9 \times 10^{-2}\,\mathrm{s}^{-1}$. To simplify the calculation, we assume the chain length in both networks is the same $n_A = n_B = 30$, and the numbers of mechanophores in both networks are equal, i.e., $c_A/c_B = 1$. We also take the applied stretch on chains as $\Lambda = 0.9\sqrt{n_B}$. In the elastic network, the applied chain force is constant during the stress–relaxation process, so that $\bar{f}_A = f_A = 38\,\mathrm{pN}$. In the relaxable network, the applied chain force decreases from a maximum value $f_B|_{t=0}$ to zero over time, so we define $\bar{f}_B = f_B|_{t=0}/2 = 19\,\mathrm{pN}$. Based on Eq. (33), we can further evaluate the time scales for chemical reaction in elastic and relaxable networks as $\tau_A^R = 119\,\mathrm{s}$ and $\tau_B^R = 49\,\mathrm{s}$. We then vary $\tau^M = \eta/N_B kT$ in the range reported for various elastomers [45,46] to investigate the effect of time scale ratio τ^M/τ_B^R on mechanical and chemical responses.

We first consider an MCR elastomer that only consists of the relaxable network (i.e., only network B or $N_A = 0$) as illustrated in Fig. 3(*a*). The mechanical relaxation and chemical reaction in this system give two time scales τ^M and τ_B^R, respectively. We investigate the responses of network B for various cases of τ^M/τ_B^R, each exhibiting a distinct reaction behavior.

When $\tau^M/\tau_B^R = \infty$, the behavior of network B approaches to the behavior of a pure elastic network, where chain forces remain constant (Fig. 3(*c*)) and activation efficiency of mechanophores increases monotonically to equilibrium (Fig. 3(*d*)). On the other hand, when the mechanical relaxation time scale is much shorter than the reaction time scale, e.g., $\tau^M/\tau_B^R = 10^{-2}$, very rapid relaxation of chain forces (Fig. 3(*c*)) prevents noticeable chemical activation (Fig. 3(*d*)) and mechanophores configuration remains unchanged throughout the test. When the two time scales are comparable to each other, e.g., $\tau^M/\tau_B^R = 1$, a small portion of mechanophores is activated and then deactivated. The activation efficiency exhibits a weak peak around time τ_B^R, after which the chain forces are significantly relaxed. When $\tau^M/\tau_B^R = 10^5$, activation response initially resembles to the case of $\tau^M/\tau_B^R = \infty$ until the activation efficiency reaches a maximum point, after which relaxation of chain forces (Fig. 3(*c*)) reveals itself by favoring the reverse reaction pathway (i.e., merocyanine to spiropyran), consequently reducing the activation efficiency of mechanophores to almost zero.

For MCR viscoelastic elastomers, represented by Fig. 3(*e*), the mechanical response and chemical reaction of the elastomer behave as a superposition of those of pure elastic and relaxable networks as shown in Figs. 3(*g*) and 3(*h*). Based on the parameters above, we can calculate $\tau_A^R/\tau_B^R = 2.4$. Next, we investigate the responses of the MCR viscoelastic elastomers with different ratios of τ^M/τ_B^R. When $\tau^M/\tau_B^R = \infty$, network B behaves as a pure elastic network for which chain forces remain constant (Fig. 3(*g*)) and activation efficiency reaches to an equilibrium plateau (Fig. 3(*h*)). When $\tau^M/\tau_B^R = 1$, chain forces in network B get relaxed (Fig. 3(*g*)) before triggering significant chemical activation in the mechanophores coupled to this network (Fig. 3(*h*)). Therefore, the activation response is mainly determined by the mechanophores in network A, which monotonically increases to equilibrium. When $\tau^M/\tau_B^R = 10^5$, the mechanical relaxation in the relaxable network (i.e., network B) is much slower than the activation of mechanophores in this network, so that the overall activation efficiency of the elastomer increases monotonically up to a maximum point. After this point, the applied force on relaxable chains ceases to favor the forward reaction over the reverse reaction, and

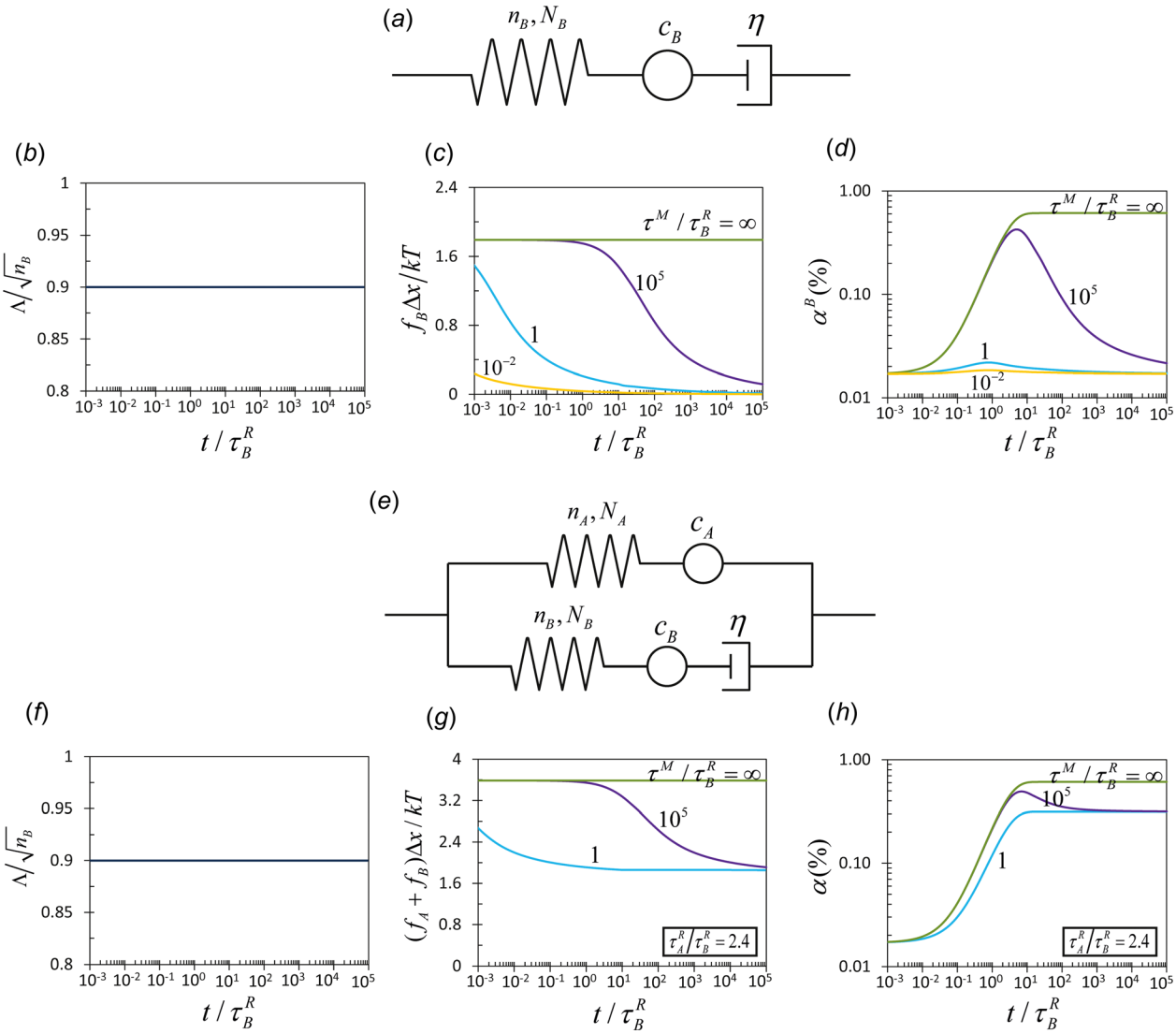

Fig. 3 A schematic of a mechanophore-coupled Maxwell element (*a*). In response to a constant stretch (*b*), the model illustrated in (*a*) varies its chain force (*c*) and activation efficiency (*d*) over time. A schematic of a mechanophore-coupled viscoelastic elastomer model (*e*). In response to a constant stretch (*f*), the model illustrated in (*e*) varies its chain force (*g*) and activation efficiency (*h*) over time.

activation efficiency declines to an equilibrium level determined by the mechanophores in the pure elastic network.

From the above examples, it is evident that the interplays of mechanical relaxation time scale τ^M and chemical reaction time scales τ_A^R and τ_B^R can lead to complicated responses of the elastomers, such as monotonic stress decrease yet nonmonotonic chemical reaction over time during a stress–relaxation test. In Sec. 4, we will use this model to characterize recent experimental data on MCR viscoelastic elastomers and address unexplained experimental observations.

4 Comparison With Experimental Results

In this section, the model developed in the current paper will be used to characterize and explain the experimental results recently reported in Ref. [25]. As a brief description of the experiment, spiropyrans were covalently linked to the center of polymethacrylate (PMA) linear chains, and the viscous behavior of this elastomer was studied at room temperature, above the glass transition temperature of 12 °C. The elastomer was subjected to uniaxial tension with various profiles of loading rates, and the stress and fluorescence intensity in the elastomer were recorded simultaneously. The activation efficiency was then assumed to be proportional to the captured fluorescence intensity, where the efficiency of a fully activated elastomer after a longtime exposure to UV irradiation was regarded as 100%. For uniaxial tension, we have $\lambda_1=\lambda$, $\lambda_2=\lambda_3=1/\sqrt{\lambda}$ in the elastomer, where λ is the applied stretch, and thus, the applied true strain is $\varepsilon=\ln\lambda$. Correspondingly, the principal Cauchy stress in the elastomer can be calculated with Eq. (17) as $\sigma_2=\sigma_3=0$ and $\sigma_1=\sigma$, where

$$\sigma=\frac{\left(\lambda^2-\frac{1}{\lambda}\right)}{3\Lambda}\left(N_An_AkT\frac{1}{\sqrt{n_A}}\beta_A+N_Bn_BkT\frac{1}{\Lambda^\nu\sqrt{n_B}}\beta_B\right) \tag{35}$$

In addition, we can divide the stress into contributions from networks A and B, respectively, i.e.

$$\sigma_A=\frac{\left(\lambda^2-\frac{1}{\lambda}\right)}{3\Lambda}N_An_AkT\frac{1}{\sqrt{n_A}}\beta_A \tag{36a}$$

$$\sigma_B = \frac{\left(\lambda^2 - \frac{1}{\lambda}\right)}{3\Lambda} N_B n_B kT \frac{1}{\Lambda^{\nu}\sqrt{n_B}} \beta_B \tag{36b}$$

The Kuhn monomer length of PMA is taken as $b = 14.7 \times 10^{-10}$ m [47] and the force-free reaction rates for spiropyran as $k^{f0} = 8.5 \times 10^{-6}\,\mathrm{s}^{-1}$ and $k^{r0} = 4.9 \times 10^{-2}\,\mathrm{s}^{-1}$ [41]. Other parameters of the model are determined by fitting it to the experimental data of stress and activation responses. We find $n_A = 30$ and $N_A = 7 \times 10^{24}$ m^{-3} from the experimental stress–strain data of the lowest rate of loading, i.e., 0.004 s^{-1} (Fig. 4(*a*)). The experimental stress–strain data of the highest rate of loading, i.e., 0.1 s^{-1} (Fig. 4(*a*)) are used to estimate $n_B = 3$, $N_B = 5.6 \times 10^{25}$ m^{-3}, and $\eta = 568\,\mathrm{MPa} \cdot \mathrm{s}$. Total number of Kuhn segments in a unit volume of elastomer is then calculated to be $n_A N_A + n_B N_B = 3.8 \times 10^{26}\,\mathrm{m}^{-3}$, which is on the same order as the reported value of 6×10^{26} m^{-3} in Ref. [25]. Moreover, the reaction distance Δx, based on the experimental results for activation efficiencies (Fig. 4(*b*)), is fitted to be 2.7×10^{-10} m, which is in the range of reaction distances previously reported [25,41].

Since the mechanophores with a total number of c are homogeneously mixed in the elastomer, we assume the number of mechanophores in each network is proportional to the volume ratio of that network as

$$c_A = c \frac{n_A N_A}{n_A N_A + n_B N_B} \tag{37a}$$

$$c_B = c \frac{n_B N_B}{n_A N_A + n_B N_B} \tag{37b}$$

From the above parameters, we can calculate $c_A / c_B = 1.25$.

This MCR elastomer is first studied under monotonic displacement loading. Figures 4(*a*) and 4(*b*) illustrate the stress–strain and chemical activation responses of the elastomer corresponding to three different stretch rates. It can be seen that the stress–strain curves predicted by the model match consistently with the experimental data (Fig. 4(*a*)). In addition, the stretch at which chemical activation becomes noticeable is in good agreement between the model and experiments (Fig. 4(*b*)). The activation stretches coincide with the stretches that induce significant stiffening of the elastomer, at which chain forces dramatically increase with stretch.

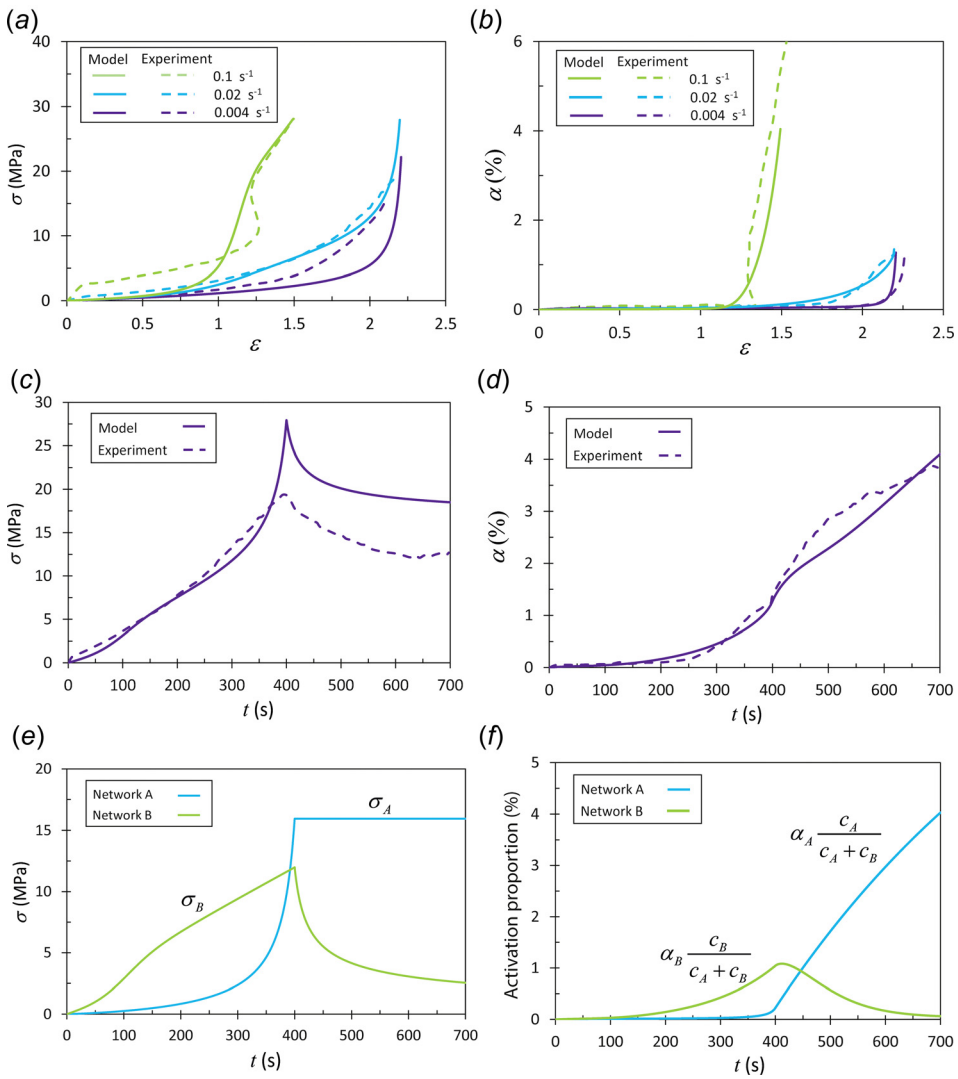

Fig. 4 Comparisons of the model's predictions with experimental results: (*a*) and (*b*) monotonic loadings at various stretch rates, (*c*) and (*d*) a monotonic loading at a stretch rate of 0.02 s^{-1} accompanied by a constant stretch of 8 held over 300 s. Time evolution of stress in networks *A* and *B* (*e*) and contribution of each network to the total activation efficiency (*f*) during the loading–relaxation process.

Next, the MCR viscoelastic elastomer is deformed to a maximum stretch of 8 with a stretch rate of 0.02 s^{-1} and then held under this constant stretch for 300 s, following the experiment reported in Ref. [25]. As the stretch increases, the principal Cauchy stress σ increases (Fig. 4(*c*)) as well as the activation efficiency (Fig. 4(*d*)). However, when the stretch is held fixed, the stress and activation efficiency do not follow the same trend. As shown in Fig. 4, when the stretch is held fixed, the stress begins to relax as expected, but the activation keeps increasing at a rate which is comparable to the rate of activation during the loading process. This nonintuitive experimental observation can be explained by our model. Considering the chain forces in networks A and B at the beginning of the relaxation process, we take $\bar{f}_A = f_A|_{t=400\,\mathrm{s}}$ and $\bar{f}_B = f_B|_{t=400\,\mathrm{s}}/2$ in Eq. (33) to calculate $\tau_A^R = 590\,\mathrm{s}$ and $\tau_B^R = 120\,\mathrm{s}$. During relaxation, while the activation efficiency of mechanophores in network B begins to decrease quickly (Fig. 4(*f*)), the activation efficiency of mechanophores in network A keeps increasing and advances to equilibrium over a time scale around τ_A^R (Fig. 4(*f*)). As a result, during the relaxation process, while the measured stress decreases over time, the total activation efficiency of the elastomer keeps increasing due to the longer reaction time scale of network A and higher portion of mechanophores in this network.

In the previous work of Silberstein et al. [25], the discrepancy between the model's predictions and experimental results was mainly attributed to the inhomogeneity within the polymer networks. From the current work, it appears that the parallel-network model illustrated in Fig. 1 can better capture this inhomogeneity. The activation efficiencies in the relaxable and elastic networks are different from each other and can be better tuned to represent the experimental results.

5 Conclusions

We developed a theoretical model to investigate the mechanochemical response of MCR viscous elastomers. The proposed model consists of mechanophore-coupled elastic and relaxable networks. It was demonstrated that the interaction between mechanical and reaction time scales and activation efficiencies of mechanophores in pure elastic and relaxable networks influence the total chemical activation response of the elastomer. The model also suggested that the increase of activation during stress relaxation of a typical MCR viscous elastomer can be understood from the ratio of reaction time scales associated with each network in our model. The proposed theoretical model is simple and general enough to represent various experimental data and observations. The model can also provide guidelines for tuning the dynamic response of a MCR elastomer via designed polymer networks. While we use a simple viscoelastic model applicable to the mode of deformation illustrated in Fig. 1(*a*), the theoretical framework presented here on coupling mechanochemical reactions of mechanophores with viscoelasticity can be readily adopted in more sophisticated models of viscoelastic elastomers for general deformation modes with multiple relaxation time scales [28,48–50].

Acknowledgment

The work is supported by NSF (No. CMMI-1253495). M. Takaffoli acknowledges The Natural Sciences and Engineering Research Council of Canada (NSERC) for the financial support.

References

[1] Melville, H. W., and Murray, A. J. R., 1950, "The Ultrasonic Degradation of Polymers," Trans. Faraday Soc., **46**(0), pp. 996–1009.
[2] Encina, M. V., Lissi, E., Sarasúa, M., Gargallo, L., and Radic, D., 1980, "Ultrasonic Degradation of Polyvinylpyrrolidone: Effect of Peroxide Linkages," J. Polym. Sci., Part B: Polym. Lett., **18**(12), pp. 757–760.
[3] Kersey, F. R., Yount, W. C., and Craig, S. L., 2006, "Single-Molecule Force Spectroscopy of Bimolecular Reactions: System Homology in the Mechanical Activation of Ligand Substitution Reactions," J. Am. Chem. Soc., **128**(12), pp. 3886–3887.
[4] Hickenboth, C. R., Moore, J. S., White, S. R., Sottos, N. R., Baudry, J., and Wilson, S. R., 2007, "Biasing Reaction Pathways With Mechanical Force," Nature, **446**(7134), pp. 423–427.
[5] Paulusse, J. M. J., and Sijbesma, R. P., 2008, "Selectivity of Mechanochemical Chain Scission in Mixed Palladium (II) and Platinum (II) Coordination Polymers," Chem. Commun., **37**, pp. 4416–4418.
[6] Li, J., Nagamani, C., and Moore, J. S., 2015, "Polymer Mechanochemistry: From Destructive to Productive," Acc. Chem. Res., **48**(8), pp. 2181–2190.
[7] Berkowski, K. L., Potisek, S. L., Hickenboth, C. R., and Moore, J. S., 2005, "Ultrasound-Induced Site-Specific Cleavage of Azo-Functionalized Poly(Ethylene Glycol)," Macromolecules, **38**(22), pp. 8975–8978.
[8] Karthikeyan, S., Potisek, S. L., Piermattei, A., and Sijbesma, R. P., 2008, "Highly Efficient Mechanochemical Scission of Silver-Carbene Coordination Polymers," J. Am. Chem. Soc., **130**(45), pp. 14968–14969.
[9] Caruso, M. M., Davis, D. A., Shen, Q., Odom, S. A., Sottos, N. R., White, S. R., and Moore, J. S., 2009, "Mechanically-Induced Chemical Changes in Polymeric Materials," Chem. Rev., **109**(11), pp. 5755–5798.
[10] Kryger, M. J., Ong, M. T., Odom, S. A., Sottos, N. R., White, S. R., Martinez, T. J., and Moore, J. S., 2010, "Masked Cyanoacrylates Unveiled by Mechanical Force," J. Am. Chem. Soc., **132**(13), pp. 4558–4559.
[11] Li, J., Shiraki, T., Hu, B., Wright, R. A. E., Zhao, B., and Moore, J. S., 2014, "Mechanophore Activation at Heterointerfaces," J. Am. Chem. Soc., **136**(45), pp. 15925–15928.
[12] Potisek, S. L., Davis, D. A., Sottos, N. R., White, S. R., and Moore, J. S., 2007, "Mechanophore-Linked Addition Polymers," J. Am. Chem. Soc., **129**(45), pp. 13808–13809.
[13] Sagara, Y., and Kato, T., 2009, "Mechanically Induced Luminescence Changes in Molecular Assemblies," Nat. Chem., **1**(8), pp. 605–610.
[14] Diesendruck, C. E., Steinberg, B. D., Sugai, N., Silberstein, M. N., Sottos, N. R., White, S. R., Braun, P. V., and Moore, J. S., 2012, "Proton-Coupled Mechanochemical Transduction: A Mechanogenerated Acid," J. Am. Chem. Soc., **134**(30), pp. 12446–12449.
[15] Davis, D. A., Hamilton, A., Yang, J., Cremar, L. D., Van Gough, D., Potisek, S. L., Ong, M. T., Braun, P. V., Martínez, T. J., White, S. R., Moore, J. S., and Sottos, N. R., 2009, "Force-Induced Activation of Covalent Bonds in Mechanoresponsive Polymeric Materials," Nature, **459**(7243), pp. 68–72.
[16] Gossweiler, G. R., Hewage, G. B., Soriano, G., Wang, Q., Welshofer, G. W., Zhao, X., and Craig, S. L., 2014, "Mechanochemical Activation of Covalent Bonds in Polymers With Full and Repeatable Macroscopic Shape Recovery," ACS Macro Lett., **3**(3), pp. 216–219.
[17] Beiermann, B. A., Kramer, S. L. B., May, P. A., Moore, J. S., White, S. R., and Sottos, N. R., 2014, "The Effect of Polymer Chain Alignment and Relaxation on Force-Induced Chemical Reactions in an Elastomer," Adv. Funct. Mater., **24**(11), pp. 1529–1537.
[18] Larsen, M. B., and Boydston, A. J., 2014, "Successive Mechanochemical Activation and Small Molecule Release in an Elastomeric Material," J. Am. Chem. Soc., **136**(4), pp. 1276–1279.
[19] Chen, Y., Zhang, H., Fang, X., Lin, Y., Xu, Y., and Weng, W., 2014, "Mechanical Activation of Mechanophore Enhanced by Strong Hydrogen Bonding Interactions," ACS Macro Lett., **3**(2), pp. 141–145.
[20] Zhang, H., Chen, Y., Lin, Y., Fang, X., Xu, Y., Ruan, Y., and Weng, W., 2014, "Spiropyran as a Mechanochromic Probe in Dual Cross-Linked Elastomers," Macromolecules, **47**(19), pp. 6783–6790.
[21] Lee, C. K., Diesendruck, C. E., Lu, E., Pickett, A. N., May, P. A., Moore, J. S., and Braun, P. V., 2014, "Solvent Swelling Activation of a Mechanophore in a Polymer Network," Macromolecules, **47**(8), pp. 2690–2694.
[22] Wang, Q., Gossweiler, G. R., Craig, S. L., and Zhao, X., 2014, "Cephalopod-Inspired Design of Electro-Mechano-Chemically Responsive Elastomers for On-Demand Fluorescent Patterning," Nat. Commun., **5**, p. 4899.
[23] Silberstein, M. N., Min, K., Cremar, L. D., Degen, C. M., Martinez, T. J., Aluru, N. R., White, S. R., and Sottos, N. R., 2013, "Modeling Mechanophore Activation Within a Crosslinked Glassy Matrix," J. Appl. Phys., **114**(2), p. 023504.
[24] Wang, Q., Gossweiler, G. R., Craig, S. L., and Zhao, X., 2015, "Mechanics of Mechanochemically Responsive Elastomers," J. Mech. Phys. Solids, **82**, pp. 320–344.
[25] Silberstein, M. N., Cremar, L. D., Beiermann, B. A., Kramer, S. B., Martinez, T. J., White, S. R., and Sottos, N. R., 2014, "Modeling Mechanophore Activation Within a Viscous Rubbery Network," J. Mech. Phys. Solids, **63**, pp. 141–153.
[26] Zhao, X., Koh, S. J. A., and Suo, Z., 2011, "Nonequilibrium Thermodynamics of Dielectric Elastomers," Int. J. Appl. Mech., **3**(2), pp. 203–217.
[27] Bergström, J. S., and Boyce, M. C., 1998, "Constitutive Modeling of the Large Strain Time-Dependent Behavior of Elastomers," J. Mech. Phys. Solids, **46**(5), pp. 931–954.
[28] Miehe, C., and Göktepe, S., 2005, "A Micro–Macro Approach to Rubber-Like Materials. Part II: The Micro-Sphere Model of Finite Rubber Viscoelasticity," J. Mech. Phys. Solids, **53**(10), pp. 2231–2258.
[29] Green, M. S., and Tobolsky, A. V., 1946, "A New Approach to the Theory of Relaxing Polymeric Media," J. Chem. Phys., **14**(2), pp. 80–92.
[30] Johnson, A. R., and Quigley, C. J., 1992, "A Viscohyperelastic Maxwell Model for Rubber Viscoelasticity," Rubber Chem. Technol., **65**(1), pp. 137–153.
[31] Zhao, X., 2012, "A Theory for Large Deformation and Damage of Interpenetrating Polymer Networks," J. Mech. Phys. Solids, **60**(2), pp. 319–332.
[32] Ronca, G., and Allegra, G., 1975, "An Approach to Rubber Elasticity With Internal Constraints," J. Chem. Phys., **63**(11), pp. 4990–4997.

[33] Flory, P. J., 1977, "Theory of Elasticity of Polymer Networks. The Effect of Local Constraints on Junctions," J. Chem. Phys., **66**(12), pp. 5720–5729.
[34] Kuhn, W., and Grün, F., 1942, "Beziehungen zwischen elastischen Konstanten und Dehnungsdoppelbrechung hochelastischer Stoffe," Kolloid-Z., **101**(3), pp. 248–271.
[35] James, H. M., and Guth, E., 1943, "Theory of the Elastic Properties of Rubber," J. Chem. Phys., **11**(10), pp. 455–481.
[36] Arruda, E. M., and Boyce, M. C., 1993, "A Three-Dimensional Constitutive Model for the Large Stretch Behavior of Rubber Elastic Materials," J. Mech. Phys. Solids, **41**(2), pp. 389–412.
[37] Evans, M. G., and Polanyi, M., 1938, "Inertia and Driving Force of Chemical Reactions," Trans. Faraday Soc., **34**(0), pp. 11–24.
[38] Hänggi, P., Talkner, P., and Borkovec, M., 1990, "Reaction-Rate Theory: Fifty Years After Kramers," Rev. Mod. Phys., **62**(2), pp. 251–341.
[39] Kramers, H. A., 1940, "Brownian Motion in a Field of Force and the Diffusion Model of Chemical Reactions," Physica, **7**(4), pp. 284–304.
[40] Bustamante, C., Chemla, Y. R., Forde, N. R., and Izhaky, D., 2004, "Mechanical Processes in Biochemistry," Annu. Rev. Biochem., **73**(1), pp. 705–748.
[41] Gossweiler, G. R., Kouznetsova, T. B., and Craig, S. L., 2015, "Force-Rate Characterization of Two Spiropyran-Based Molecular Force Probes," J. Am. Chem. Soc., **137**(19), pp. 6148–6151.
[42] Bell, G. I., 1978, "Models for the Specific Adhesion of Cells to Cells. A Theoretical Framework for Adhesion Mediated by Reversible Bonds Between Cell Surface Molecules," Science, **200**(4342), pp. 618–627.
[43] Khan, S. A., Prud'homme, R. K., and Larson, R. G., 1987, "Comparison of the Rheology of Polymer Melts in Shear, and Biaxial and Uniaxial Extensions," Rheol. Acta, **26**(2), pp. 144–151.
[44] Isono, P. D. Y., Kamohara, T., Takano, A., and Kase, T., 1997, "Nonlinear Viscoelastic Properties and Change in Entanglement Structure of Linear Polymer," Rheol. Acta, **36**(3), pp. 245–251.
[45] Tobolsky, A. V., 1956, "Stress Relaxation Studies of the Viscoelastic Properties of Polymers," J. Appl. Phys., **27**(7), pp. 673–685.
[46] Curro, J. G., and Salazar, E. A., 1975, "Physical and Chemical Stress Relaxation of Elastomers," J. Appl. Polym. Sci., **19**(9), pp. 2571–2581.
[47] Fetters, L. J., Lohse, D. J., and Colby, R. H., 2007, "Chain Dimensions and Entanglement Spacings," *Physical Properties of Polymers Handbook*, Springer, New York, pp. 447–454.
[48] Guo, J., Xiao, R., Park, H. S., and Nguyen, T. D., 2015, "The Temperature-Dependent Viscoelastic Behavior of Dielectric Elastomers," ASME J. Appl. Mech., **82**(9), p. 091009.
[49] Park, H. S., and Nguyen, T. D., 2012, "Viscoelastic Effects on Electromechanical Instabilities in Dielectric Elastomers," Soft Matter, **9**(4), pp. 1031–1042.
[50] Henann, D. L., and Bertoldi, K., 2014, "Modeling of Elasto-Capillary Phenomena," Soft Matter, **10**(5), pp. 709–717.